EXPLORING HIGH ENERGY ACTIVITIES IN THE SUPERBUBBLE N44 WITH XMM-$NEWTON$

H. Nakajima[1], H. Yamaguchi[1], M. Ueno[2], A. Bamba[3], and K. Koyama[1]

[1]Department of Physics, Graduate School of Science, Kyoto University, Sakyo-ku, Kyoto, Japan
[2]Department of Physics, Tokyo Institute of Technology, Ohokayama, Meguro, Tokyo, Japan
[3]RIKEN (Institute of Physical and Chemical Research), Hirosawa, Wako, Saitama, Japan

ABSTRACT

We report the results of the XMM-$Newton$ Observation of N44, one of the brightest Superbubble (SB) in X-rays in the Large Magellanic Cloud. There is a significant X-ray emission inside the main shell, blowout regions, and supernova. We discovered the spatial structure of inner hot gas; The inner hot gas consists of high temperature ($\sim$1.8 keV) and low temperature ($\sim$0.6 keV) components. This value is exceedingly high compared with other SBs. Because the former shows significantly lower ionization parameter than the latter, this component is due to recent supernovae. In the vicinity of OB-type stars, abundance of hot gas is significantly higher than other regions and temperature is consistent with typical plasma surrounding OB-type stars. These features strongly support that we detect the contribution from stellar winds to the hot gas inside the bubble.

Key words: individual(N44); Superbubble; X-rays.

1. INTRODUCTION

Massive stars are formed in groups by the collapse of molecular clouds. Because of their short lifetimes of 3–20 Myr (Schaller et al., 1992) and small dispersion velocities of 4–6 km s^{-1} (Blaauw , 1991; Mel'nik & Efremov, 1995), supernova (SN) progenitors remain and explode close to their birth place. Following SN explosions may occur in the cavity formed by preceding ones and/or strong stellar winds from OB-type stars. Large hot cavities formed by these process is called Superbubbles (SBs).

In an SB, successive SN re-heat and changes the chemical evolution of of the hot gas and swept ISM (soft thermal X-rays). The study of soft thermal X-rays provides key information on the hot ($\geq 10^6$K) shock-heated gas in the SB. An excess of diffuse X-ray emission in SBs indicates the presence of interior supernova remnants (SNRs) shocking the inner walls of the SB shell (Chu & Mac Low , 1990; Wang & Helfand , 1991; Dunne et al., 2001). Young massive stars in the OB association are also known to be moderately bright X-ray sources. Therefore X-ray observations on SBs provide valuable information on the overall structure and evolution of them.

We also expect that accelerated particles in the shock drive into molecular clouds, depositing energy (hard non-thermal X-rays). The discovery of power-law (non-thermal) X-rays from SN 1006 (Koyama et al., 1995) indicate the existence of extreme high energy charged particles accelerated up to the knee energy by the first order Fermi process. These breakthrough studies of cosmic ray origin from shell-like SNRs lead a successive discovery of new class of shell-like SNRs (hereinafter, we call those SNRs as "SN 1006-like SNRs", or "SN 1006s" in short), such as G347.3$-$0.5 (Koyama et al., 1997; Slane et al., 1999; Muraishi et al., 2000), RCW 86 (Bamba et al., 2000; Borkowski et al., 2001), G266.2$-$1.2 (Slane et al., 2001), and G28.6$-$0.1 (Ueno et al., 2003). Furthermore even in the typical shell-like SNRs which are dominated by thermal X-rays also emit non thermal X-rays (e.g. Cas A, Tycho). Thus virtually all the young (less than 1000 years) shell-like SNRs, more or less, may emit non-thermal X-rays. It is conceivable that SBs also emit non-thermal X-rays, because SBs are created by the combined action of stellar winds and SN explosions of massive stars in an OB association.

Systematic X-ray observations on SBs have only been made by $Einstein$, $ROSAT$, and $ASCA$. The energy band of the formers is limited only in the soft band and the data of the latter has a poor statistics, hence soft X-ray spectrum/morphology as well as the question whether or not the SBs have hard X-ray tail is not yet available. Unresolved X-ray peaks superposed on the diffuse X-ray emission may also indicate the existence of stellar X-ray sources in the SBs.

The Large Magellanic Cloud (LMC) is an ideal laboratory for the observation of SBs in the X-ray band. Because we know the distance to the LMC as 50 kpc with small uncertainty (Feast , 1999), we are able to derive diameter of SBs (1 pc = 4 arcsec). Since the LMC is a faceon galaxy located at high galactic latitude, the absorption through the Galaxy and in the LMC can be small in the relevant X-ray band. Furthermore, the LMC has numbers of SBs. The systematic study in the X-ray band has been done with $ROAST$ (Dunne et al., 2001). Including the archive data sets with $ASCA$ and high resolution H_α images, we can do systematic X-ray study with less bias than in other galaxies.

N44 is one of the brightest HII regions in the LMC, consisting of three OB associations (Henize , 1956; Lucke & Hodge , 1970). and a SB with a size of $\sim$100 pc $\times$ 75 pc. Meaburn & Laspias (1991) detected the expansion of the two large shells DEM L140 and DEM L152, confirmed that these are SBs. In the X-ray band, the diffuse X-ray emission from N44 is detected by $EinsteinObservatory$ (Chu & Mac Low , 1990; Wang & Helfand , 1991). With the following $ROSAT$ observation (Chu et al., 1993; Magnier et al., 1996; Dunne et al., 2001), diffuse X-ray emission well correlated with Hα emission was detected. The temperature of inner hot gas was higher than other SBs (Dunne et al., 2001), by which we've been expected the detection of non-thermal X-rays from N44.

In this paper, after describing the observation and data reduction (Section 2), we report the results of the image and spectral analysis of the main shell (Section 3). Then we discuss the energy balance and some other features (Section 4) and summarize this paper (Section 5).

2. OBSERVATION AND DATA REDUCTION

N44 was observed with The European Photon Imaging Camera (EPIC) onboard XMM-$Newton$ on the 2004 December 4–5. The exposure time was $\sim$50 ks. The telescope optical axis position on the EPIC was R.A. = $05^{\rm h}22^{\rm m}20\overset{\rm s}{.}00$, Decl.= $-67°56'40\overset{''}{.}0$ (J2000). Thanks to the large FOV ($30'$ of diameter), whole region of N44 including nearby SNR was covered. We used the ODF data provided by the XMM-$Newton$ Science Operations Centre.

For the data reduction, we used $emchain$ and $epchain$ in the analysis software SAS version 6.5.0 with the bad pixel finding algorithm on. Then we cut the events in the duration of background flare with the following way. First we made light curves of the Pattern 0 events in the energy band of 10–15 keV with the 100 sec binning and made histogram of the count rate. Then we fit the distribution of count rate with gauss function and cut the duration in which the count rate is higher with 2σ significance than the gaussian peak. Second we did the same cutting but using the events detected in the region of $>12'$ from the center of FOV in the energy band of 1.0–5.0keV and Pattern $<$12 for MOS and $<$4 for pn chip. Then the effective exposure time was then $\sim$23 ks for MOS and $\sim$17 ks for pn chip.

Hereafter, we used those events that has Pattern $<$ 12 for MOS, $<$4 for pn chip in order to eliminate the events due to charged particles and hot and flickering pixels.

3. DATA ANALYSIS

3.1. Image Analysis

Figure 1 shows soft (0.2–2.0 keV) and hard (2.0–7.0 keV) band X-ray image of N44. As is is proved in the past X-ray observation, the distribution of the X-ray emission has clear correlation with that of Hα (Magnier et al., 1996).

In the soft band, there is an almost uniform X-ray emission from entire region of main shell, some blowout regions, and the nearby SNR 0523–67.9. However in the hard band, there seems to be no significant diffuse emission in the main shell and blowout regions. This feature is obviously different from that was seen in 30 Dor C (Bamba et al., 2004).

We conducted the point source search with $eboxdetect$ and $emldetect$ command in SAS 6.5.0 in the soft (0.2–2.0 keV) and hard (2.0–7.0 keV) energy band. The detection minimum likelihood was 6 for $eboxdetect$ and 10 for $emldetect$. In the hard band, we detected 13 sources from the surrounding region of the main shell (1). Although we detected many sources in the soft band from entire region of the main shell uniformly, it is unreasonable to confirm them as real point sources, then we rejected them.

3.2. Spectral Analysis of main shell

The Galactic absorption column was estimated using the H I data by Dickey & Lockman (1990) as $N_{\rm H,HI}$ = 6.35 $\times$ 10^{20} cm^{-2}. Arabadjis & Bregman (1999) reported that the value of $N_{\rm H}$, measured in the X-ray band, is twice that of $N_{\rm H,HI}$ in the case of $|$b$|$ $>$ 25deg; and $N_{\rm H} > 5 \times 10^{20}$ cm^{-2}. Therefore, we fixed the galactic absorption column to be $N_{\rm H}$ = 1.27 $\times$ 10^{21} cm^{-2}; we used the cross sections of Morrison & McCammon (1983) and the solar abundances of Anders & Grevesse (1989). The absorption column in the LMC was, on the other hand, treated as a free parameter with the mean LMC abundance (Russel & Dopita, 1992; Hughes et al., 1998).

Figure 2 shows the spectrum of MOS 1 and 2 chip extracted from the entire main shell region. We tested thin thermal and composite (thermal and non-thermal) plasma model in the spectral fit. In the case of the latter model, fit result was statistically rejected (χ^2/d.o.f. = 314.80/161) while the former model well reproduce the spectrum (χ^2/d.o.f. = 188.24/161). The fitting parameters are shown in Table 1.

We then further divide main shell into three regions: northwest, southeast, and the region in which OB-type

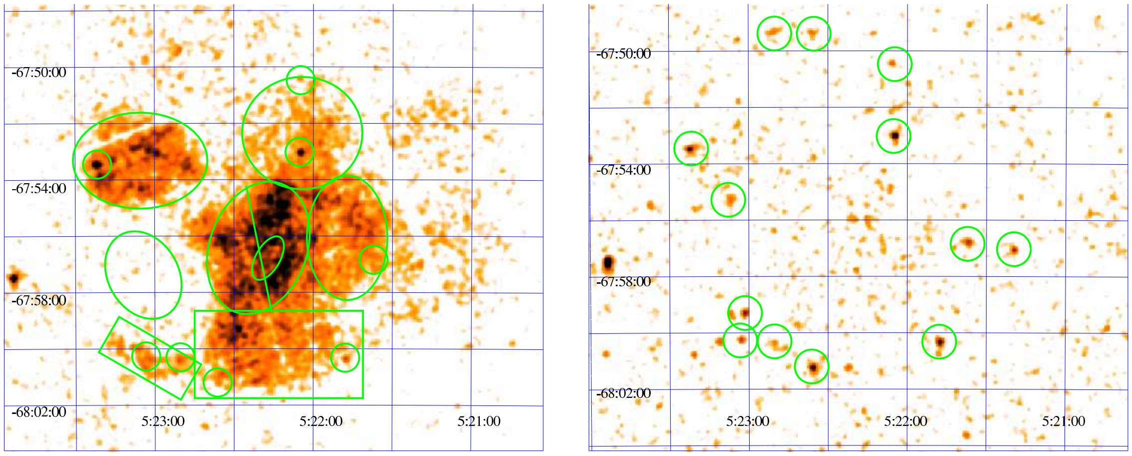

Figure 1. Soft (0.2–2.0 keV) and hard (2.0–7.0 keV) band X-ray image of N44. The regions from which we extracted photons are shown in the soft band image. The main shell are divided into northwest and southeast regions. Hereafter we concentrate our study on the main shell. In the hard band image we show the point sources detected in the band.

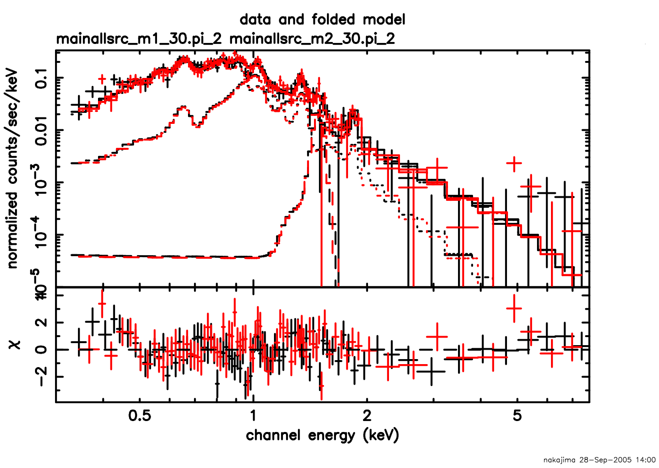

Figure 2. Background-subtracted spectrum extracted from entire main shell region. We fit this spectrum with thin thermal plasma model with two temperature. Al fluorescence line is also considered.

stars are concentrated like Figure 1. The energy spectra from formers are shown in Figure 3 and their fitting parameters are presented in Table 1. Northwest region shows the high temperature feature seen in Figure 2 and significantly low ionization parameter than southeast region.

The plasma temperature seen in the northwest region is exceedingly high compared with other SBs (Naze et al., 2004; Cooper et al., 2004; Bamba et al., 2004). This feature suggests that N44 is the most active, that is, experienced the latest SN among these SBs.

3.3. Spectral Analysis of vicinity of OB-type stars

Oey & Massey (1995) and Will et al. (1997) have observed OB associations LH47, which is located inside the main shell and its surrounding regions with optical light.

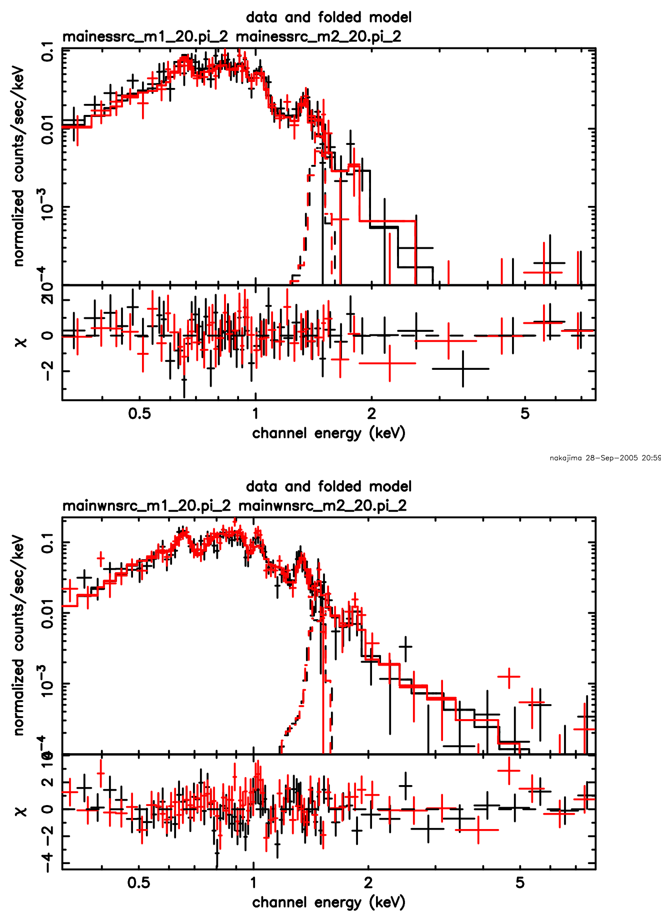

Figure 3. Background-subtracted spectrum extracted from northwest and southeast region of main shell (upper and lower panel, respectively). Al fluorescence line is also considered.

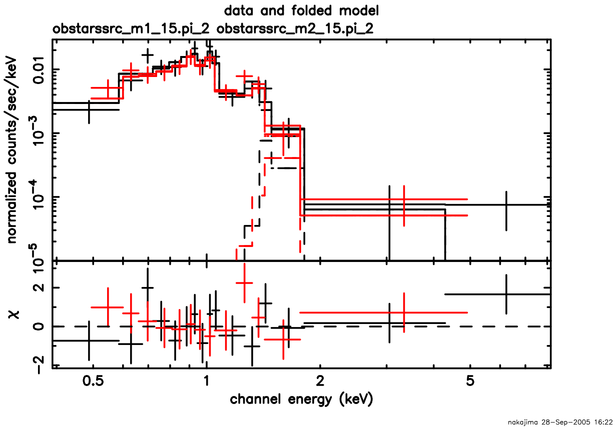

Figure 4. Background-subtracted spectrum extracted from vicinity of OB-stars association LH 47. Al fluorescence line is also considered.

Oey & Massey (1995) investigated spectroscopic data of the 62 bluest stars ($> 10\mathrm{M}_\odot$)in the LH47/48, and derived the spectral types of 54 stars in LH 47. Will et al. (1997) also took spectra of V band brightest 14 stars and got almost consistent spectral types of them. On the whole, OB-type stars are concentrated at center of main shell, inside the westside shell, HII region N44B and N44C which are located at southwestern outside of the main shell.

Hence we defined the regions from which we extract the photons like in Figure 1 and got the spectrum shown in Figure 4 and fitting parameters presented in Table 1. Furthermore in the case of this region, we set the abundance of O, Ne, and Mg to be free. Then we got the abundance of 0.46 (>0.10), 1.15 (>0.26), 0.91 (>0.21), respectively.

4. DISCUSSION

4.1. Energy Balance of N44

Utilizing the thermal energy derived in 3.2, we investigate the energy balance in the case of N44.

For the amount of energy injection to SB, the combined action from SN and stellar winds from OB-type stars must be considered. Oey & Massey (1995) derived the approximate age of LH 47 from the initial mass function of members to be $\sim$10 Myr, then the integral of mechanical luminosity of stellar wind from OB stars and SN explosion are $\sim 3\times10^{51}$ ergs and $\sim$1–4×10^{51} ergs respectively.

On the other hand, the amount of energy ejection can be estimated by measuring the thermal energy of hot gas in the SB and kinetic energy of HI and HII shell. Kim et al. (1998) estimated the latters to be $\sim 2.4\times10^{50}$ ergs and $\sim 5.0\times10^{49}$ ergs respectively, which is negligible compared with SN explosion energy. Thermal energy inside the main shell, which can be calculated from flux, is $2.62\times10^{51}\sqrt{\epsilon}$ ergs (where the ϵ is filling factor). Furthermore we also derived the flux and thermal energy from blowout region and western another shell (Figure 1). The sum of the thermal energy is $2.15\times10^{51}\sqrt{\epsilon}$ ergs. Then the total thermal energy is $4.77\times10^{51}\sqrt{\epsilon}$ ergs, which reaches to the total injected energy.

This feature shows a clear contrast against N51D, another SB in the LMC. In the case of N51D, approximately two third of the injected energy is missing (Cooper et al., 2004) which means a significant fraction of the stellar mechanical energy must have been converted into other forms of energy. The X-ray spectrum of the diffuse emission from N51D requires a power-law component to explain the featureless emission at 1.0–3.0 keV. The origin of this power-law component is unclear, but it may be responsible for the discrepancy between the stellar energy input and the observed interstellar energy in N51D. In the case of N44, no significant diffuse non-thermal emission possibly corresponds to the negligible amount of missing energy. The case dependency of the amount of the missing energy have to be investigated more detail comparing our X-ray dataset with data of other bands.

4.2. The contribution from OB-type stars to the hot gas?

In the typical case of X-ray emission from OB-type stars, the temperature of hot plasma is <1.0 keV and the solar abundance. The hot plasma in the vicinity of OB-type stars shows quite a similar feature; the abundance of Ne and Mg is similar to the solar value, while other region inside the main shell show consistent results with the mean LMC value of 0.3. According to the catalog in the Oey & Massey (1995), there are at least 4 O-type stars and 5 B-type stars in this region. On the other hand the absorption corrected flux in the energy band of 0.2–2.0 keV is 1.49×10^{-13} ergs cm^{-2} s^{-1} which corresponds to the luminosity of 4.50×10^{34} ergs s^{-1}. Considering the luminosity of galactic O-type stars (Babel & Montmerle, 1997), this value is not too large because there must be some contamination from diffuse hot gas which fills entire shell. Hence we possibly first detect the contribution from OB-type stars to the hot gas in an SB separately from that of SNRs.

5. CONCLUSION

We report the results of the *XMM-Newton* Observation of N44, one of the brightest Superbubble (SB) in X-rays in the Large Magellanic Cloud. There is a significant X-ray emission inside the main shell, blowout regions, and supernova as seen in the past X-ray observations. We summarize our new results as follows.

(1)We detected several point sources inside blowout regions and western shell, which is to be further investigated.

Table 1. Fitting parameters for each region.

Region	$N_{\rm H}$† ($\times 10^{21}$Hcm^{-2})	kT† (keV)	τ† ($\times 10^{10}$ sec cm^{-3})	flux‡	χ^2/d.o.f.
Entire Main Shell					
(low kT component)	2.92 (2.42–3.46)	0.6(0.4–0.8)	2.5 (1.9–3.8)	3.51	188.24/153
(high kT component)	–	2.2(1.5–2.5)	5.3 (4.6–7.0)	–	–
North-West	2.40 (1.51–3.03)	1.8 (1.7–1.9)	1.4 (1.1–1.7)	1.30	180.94/139
South-East	1.00 (0.73–1.19)	0.40 (0.39–0.43)	9.1×10^1 (6.8×10^1–2.4×10^2)	0.35	72.37/95
Vicinity of OB-stars	1.81 (<2.20)	0.40 (0.32–0.64)	8.2×10^2 (4.8×10^1–5.0×10^3)	0.12	21.72/20

† The 90% confidence regions are in the parentheses.

‡ Absorption corrected flux in the 0.5–7.0 keV band ($\times10^{-12}$ ergs cm^{-2} s^{-1}).

(2)We discovered the spatial structure of inner hot gas; The inner hot gas consists of high temperature plasma of kT = 1.8 (1.7–1.9) keV and low temperature plasma of kT = 0.40 (0.39–0.43) keV. This value is exceedingly high compared with other SBs. Because the former shows significantly lower ionization parameter than the latter, this component is due to recent supernovae.

(3)In the vicinity of OB-type stars, abundance of hot gas is significantly higher than other regions and temperature is consistent with typical plasma surrounding OB-type stars. These features strongly support that we detect the contribution from stellar winds to the hot gas inside the bubble.

ACKNOWLEDGMENTS

H. N. and H. Y. are supported by JSPS Research Fellowship for Young Scientists.

REFERENCES

Anders E., & Grevesse N. 1989, Geochim. Cosmochim. Acta, 53, 197

Arabadjis J. S., & Bregman J. N. 1999, ApJ, 510, 806

Babel J. & Montmerle T. 1997, ApJ, 485, L29

Bamba A., Koyama K., & Tomida H. 2000, PASJ, 52, 1157

Bamba A., Ueno M., Nakajima H., & Koyama K. 2004, ApJ, 602, 257

Blaauw A. 1991, in the Physics of Star Formation and Early Stellar Evolution, NATO Advanced Science Institutes (ASI) Ser. C, ed. C. J. Lada & N. D. Kylafis (Kluwer: Dordrecht), 342, 125

Borkowski K. J., Rho J., Reynolds S. P., & Dyer K. K. 2001, ApJ, 550, 334

Chu Y.-H. & Mac Low M.-M. 1990, ApJ, 365, 510

Chu Y.-H., Mac Low M.-M., Garcia-Segura G., Wakker B. & Kennicutt R. C. 1993, ApJS, 414, 213

Cooper R. L., Guerrero M. A., Chu Y.-H., Chen C.-H. R., & Dunne B. C. 2004, ApJ, 605, 751

Dickey J. M., & Lockman F. J. 1990, ARA&A, 28, 215

Dunne B. C., Sean D., Points S. D., & Chu Y.-H. 2001, ApJS, 136, 119

Feast M. 1999, PASP, 111, 775

Henize, K. G. 1956, ApJS, 2, 315

Hughes J. P., Hayashi I., & Koyama K. 1998, ApJ, 505, 732

Kim S., Chu Y.-H., Staveley-Smith L., Smith R. C. 1998, ApJ, 503, 729

Koyama K., Petre R., Gotthelf E. V., Hwang U., Matsuura M., Ozaki M., & Holt S. S. 1995, Nature, 378, 255

Koyama K., Kinugasa K., Matsuzaki K., Nishiuchi M., Sugizaki M., Torii K, Yamauchi S., & Aschenbach B. 1997, PASJ, 49, L7

Lucke P. B. & Hodge P. W. 1970, AJ, 75, 151

Magnier E. A., Chu Y.-H., Points S. D., Hwang U., & Smith R. C. 1996, ApJ, 464, 829

Meaburn J. & Laspias N. V. 1991, A&A, 245, 635

Mel'nik A. M., & Efremov Y. N. 1995, Astron. Lett., 21, 10

Morrison R., & McCammon D. 1983, ApJ, 270, 119

Muraishi H., Tanimori T., Yanagita S., et al. 2000, A&A, 354, L57

Nazé Y., Antokhin I. I., Rauw G., Chu Y.-H., Gosset E., & Vreux J.-M. 2004, A&A, 418, 841

Oey M. S. & Massey P. 1995, ApJ, 452, 216

Russel S. C., & Dopita M. A. 1992, ApJ, 384, 508

Schaller G., Schaerer D., Meynet G., & Maeder A. 1992, A&AS, 96, 269

Slane P., Gaensler B. M., Dame T. M., Hughes J. P., Plucinsky P. P. & Green A. 1999, ApJ, 525, 357

Slane P., Hughes J. P., Edgar R. J., Plucinsky P. P., Miyata E., Tsunemi H., & Aschenbach B. 2001, ApJ, 548, 814

Ueno M., Bamba A., Koyama K., & Ebisawa K. 2003, ApJ, 588, 338

Wang Q. & Helfand D. J. 1990, ApJ, 373, 497

Will J.-M., Bomans D. J., & Dieball A. 1997, A&AS, 123, 455